Power Electronic Systems
Laboratory

IEEE Transactions on Industry Applications, Vol. 49, No. 4, pp. 1515-1522, July/August 2013

Stator Tooth Design Study for Bearingless Exterior Rotor PMSM

T. Reichert,
J. W. Kolar,
T. Nussbaumer

Eidgenössische Technische Hochschule Zürich
Swiss Federal Institute of Technology Zurich

Stator Tooth Design Study for Bearingless Exterior Rotor PMSM

Thomas Reichert, *Student Member, IEEE*, Johann W. Kolar, *Fellow, IEEE*, and Thomas Nussbaumer, *Member, IEEE*

***Abstract*—This paper describes important design considerations for a bearingless brushless motor (permanent magnet synchronous motor, PMSM) in exterior rotor construction. In order to come up with a compact energy-dense setup which can provide both bearing forces and high torque, several parameters have to be accounted for while considering mutual dependences. Moreover, the magnetic bearing and the drive are interlinked for this disk-shaped bearingless motor (with combined concentrated windings). A detailed analysis about the design of the stator teeth has been undertaken, and the influence on torque and active and passive radial forces has been investigated.**

***Index Terms*—Bearingless motor, brushless motor, exterior rotor, motor design, self-bearing motor.**

I. Introduction

IN VARIOUS industrial processes of fluid handling, a sealed chamber is required to separate the process liquid from the environment [1], [2]. In particular, for high-purity applications or in the case of hazardous process substances, a reliable separation has to be guaranteed. However, most of the processes depend on interactions of the process liquid with its surroundings. One of the most prominent steps in an industrial process is the application of a rotational force to the liquid (e.g., mixing and pumping). For this purpose, the rotational force has to be transmitted into the sealed chamber from an electrical motor outside of the process room. Moreover, the rotating component part inside the process room needs to be supported with some type of bearing.

Several solutions already exist for this application, but they all suffer from certain drawbacks. The rotational force could be passed into the process chamber using a sealed opening. However, no seal is completely leakproof, wherefore it is not suitable for hazardous liquids. Moreover, particles are generated that impact high-purity applications. Alternative implementations with magnetic couplings avoid an opening in the process chamber. With this solution, however, an additional bearing (usually some type of sliding contact bearing) is required inside the process room, which is unfavorable for high purity as well. An additional drawback of both solutions emerges for applications with delicate process liquids, such as bioreactor applications. Seals, magnetic couplings, and additional bearings lead to pinchoff areas that cam harm the process fluid or solid particles inside the tank (e.g., blood or cell cultures) [3].

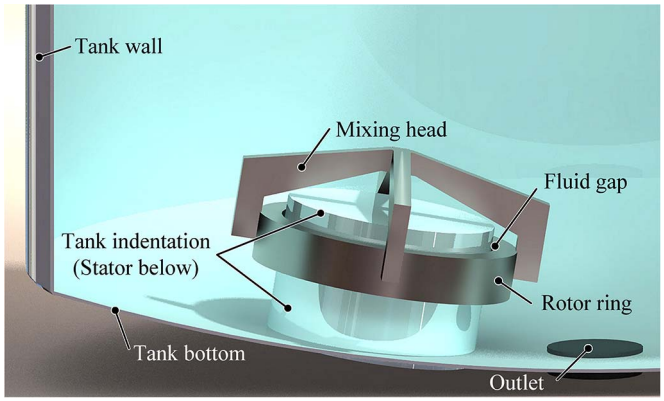

Fig. 1. Setup of a bearingless exterior rotor motor implemented for mixing applications. The stator is buried below a tank indentation. With this measure, only the levitated rotor (with the mixing head) is inside the tank. There is a fluid gap between the rotor ring and the tank indentation.

With a bearingless brushless motor [4]–[9], all the aforementioned disadvantages can be overcome. This motor type consists of a magnetic bearing, which is integrated into the magnetic circuit of the drive. Therefore, a very compact setup can be achieved, and due to the contactless manner of force transmission for both bearing and drive, the problems of particle contamination and pinchoff areas are eliminated. As an additional benefit, the absence of wear promises a longer lifetime and less maintenance cost.

This paper focuses on a disk-shaped bearingless brushless motor PMSM with an exterior rotor (see Fig. 1), with passive stabilization of the axial and the tilting position. The rotor itself is encapsulated and connected with the mixing head. It is the only component that is placed inside the process room. The stator is installed below a tank indentation and connected to the power and control unit outside of the tank. Using this exterior rotor construction type, high torque can be achieved while the rotational speed will be in a moderate range (up to 500 r/min). This bearingless motor is highly qualified for high-purity mixing applications, or it can be directly integrated into a bioreactor, building a bearingless agitator. Such an agitator would reduce cell destruction because of the large magnetic gap resulting in the absence of pinchoff areas. Furthermore, the large magnetic gap facilitates cleaning-in-place

Manuscript received July 3, 2012; revised September 27, 2012; accepted November 21, 2012. Date of publication April 12, 2013; date of current version July 15, 2013. Paper 2012-EMC-420.R1, presented at the 2011 IEEE Energy Conversion Congress and Exposition, Phoenix, AZ, USA, September 17–22, and approved for publication in the IEEE Transactions on Industry Applications by the Electric Machines Committee of the IEEE Industry Applications Society.

T. Reichert and J. W. Kolar are with the Power Electronic Systems Laboratory, Swiss Federal Institute of Technology (ETH) Zurich, 8092 Zurich, Switzerland (e-mail: reichert@lem.ee.ethz.ch; kolar@lem.ee.ethz.ch).

T. Nussbaumer is with Levitronix GmbH, 8005 Zurich, Switzerland (e-mail: nussbaumer@levitronix.com).

Color versions of one or more of the figures in this paper are available online at http://ieeexplore.ieee.org.

Digital Object Identifier 10.1109/TIA.2013.2257975

and sterilization-in-place applications [10]. Owing to these benefits, additional implementation costs and an increased control effort are outweighed.

Over the last few years, several novel bearingless topologies have been introduced, and their properties have been discussed. For the rotor, consequent-pole [9], [11], [12], multi-consequent-pole [13] or multipole [2], [5], [6] arrangements can be distinguished. For the stator, new approaches with segmented elements [2], [6] or a pole distribution into main and supplemental poles [13] have been investigated. For most of these topologies, design optimizations for a specific setup were carried out. Usually, either closed pole shoes known from traditional machine theory or bar-shaped stator teeth have been chosen. However, no thorough investigation has been presented in the literature so far which investigates the design of the stator tooth with its tooth tip (pole shoes) and its influence on both torque and bearing forces for the bearingless drive.

In this paper, the focus lies on a more general and profound design study for the bearingless motor technology with an emphasis on the stator tooth design. For this study, the topology of a bearingless motor in exterior rotor construction has been chosen. The four-slot [14] and six-slot [15] topologies of this motor concept have already been presented, and the design optimization for specific topologies has been undertaken. Moreover, the control of this bearingless motor with concentrated (each coil entirely wound around a single stator tooth) combined (one single coil per stator tooth and each coil contributing to both torque and bearing force generation) windings has been explained [16]. Additionally, application-specific properties (e.g., for an installation in a bioreactor) such as thermal and fluid-dynamic behavior have been addressed [17].

This paper takes a more general approach with a broad design study of a bearingless motor, which helps the reader to identify relevant design decisions and their impact on the motor performance. In Section II, the design parameters are presented, and their interdependences are discussed. Particular attention is given to the design of the stator teeth and the tooth tips with a detailed analysis presented in Section III, where the influence on the torque and the passive and active radial forces in dependence on the stator tooth shape is derived and discussed. Finally, in Section IV, a test setup is presented to confirm the results of the analysis.

II. Design Parameters for Bearingless Motors

The design of a bearingless motor is a complex task because several factors influence each other. Moreover, some of the design goals contradict each other (see Section III). For the targeted application, high torque has to be achieved, and high priority is given to this requirement in the design. Additionally, the bearing forces need to be sufficiently large in order to levitate the rotor permanently during operation.

For this purpose, according to Ooshima *et al.* [9], both passive reluctance forces as well as active radial bearing forces have to be considered in the design.

For the design analysis in this paper, a topology with a stator consisting of six stator teeth has been chosen. It is surrounded by the rotor, which is built of 16 radially magnetized permanent magnets and a back iron ring [16]. The axial and the tilting position are stabilized passively by means of attracting reluctance forces between the rotor magnets and the stator iron. The radial rotor position is also influenced by this passive reluctance force. In this case, however, there is no stable working point, and an active radial bearing has to be implemented. It is realized with the six concentrated coils and superimposed to the drive control. This means that, with all six coils, radial bearing forces and drive torque are generated simultaneously.

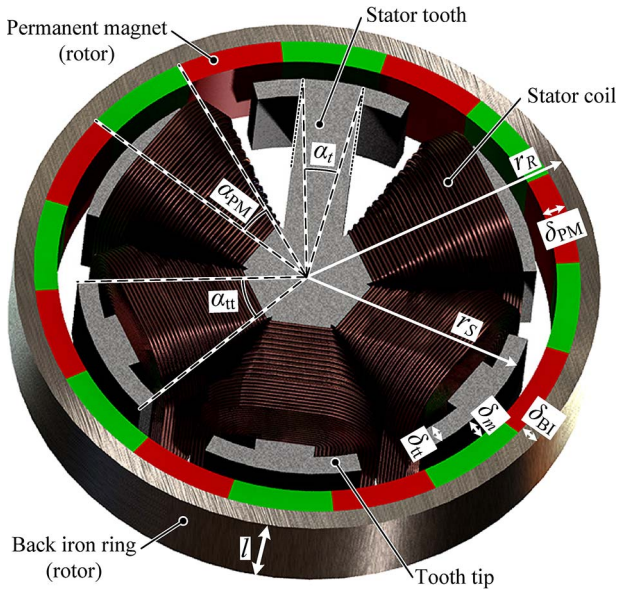

Fig. 2. Geometric design parameters of the bearingless brushless motor with a ring-shaped exterior rotor. The exemplary topology consists of six stator teeth and 16 permanent magnets. One coil has been omitted for better visibility.

Fig. 2 shows the geometric design parameters for this bearingless motor. There are five parameters that define the radial dimensions. The outer rotor radius r_R determines the overall motor size. The available space is then split into the rotor, the magnetic gap δ_m, and the stator inside the hollow rotor. For the rotor, the back iron δ_{BI} and the magnet thicknesses δ_{PM} have to be determined, which will also determine the inner rotor radius. In order to achieve high torque, the rotor should be chosen narrow (leading to a large radius of the magnetic gap, which is the lever arm of the motor). However, the permanent magnets have to provide a certain magnetic flux passing through the gap in order to achieve large active and passive forces. Therefore, a certain minimum required magnet thickness (usually in the range of the magnetic gap) is necessary, which then defines the lower limit for the back iron thickness in order to avoid the saturation of the iron. If the inner rotor radius is set, either the magnetic gap thickness or the outer stator radius r_S can be chosen because these values now depend on each other (see Table I). For the targeted application, the magnetic gap thickness is rather large in the range of 4%–8% of the overall motor radius because the sealed chamber has to be installed through this gap. Finally, for the stator, the radial thickness of the tooth tip δ_{tt} has to be chosen (see Section III). The remaining (nonradial) geometric parameters determine the motor height (or length, respectively) l and the geometric shape of the stator teeth. Table I gives an overview

TABLE I
DESIGN PARAMETERS

Parameter	Symbol	Normalized value
Stator slot number	q	
Pole pair number	p	$[f(q)]$[a]
Outer rotor diameter	r_R	
Maximum allowed current density	$J_{\max}$	
Permanent magnet angle	α_{PM}	$[\,360°/2p\,]$
Magnetic gap thickness	δ_m	$f_m = \delta_m / r_R$
Permanent magnet thickness	δ_{PM}	$f_{\mathrm{PM}} = \delta_{\mathrm{PM}} / r_R$
Back iron thickness	δ_{BI}	$f_{\mathrm{BI}} = \delta_{\mathrm{BI}} / r_R$
Stator tooth angle	α_t	$n_t = \alpha_t / \alpha_{\mathrm{PM}}$
Tooth tip angle	α_{tt}	$n_{\mathrm{tt}} = \alpha_{\mathrm{tt}} / \alpha_{\mathrm{PM}}$
Tooth tip thickness	δ_{tt}	$f_{\mathrm{tt}} = \delta_{\mathrm{tt}} / r_R$
Motor height	l	$n_l = l / r_R$
Stator radius	r_S	$[\,r_R - (\delta_{\mathrm{BI}} + \delta_{\mathrm{PM}} + \delta_m)\,]$
Slot fill factor	k_{coil}	0.5 (fixed)

a. The pole pair number is dependent on the slot number, because only certain pole/slot combinations are allowed for a bearingless motor construction [11].

of the considered design variables. In order to allow for scalable design considerations, the geometric variables are set in relation to two independent variables, namely, the outer rotor radius r_R and the magnet angle α_{PM}. (The latter is actually given once the pole pair number was chosen.) The remaining geometric variables can then be expressed as a fraction of these two independent variables, with factors f (where $0 < f < 1$) and n (where $n > 0$).

Apart from the geometric variables, there is one more important design parameter, namely, the maximum allowed current density $J_{\max}$ in the stator coils. It can be chosen independently of the geometric variables. However, it is influenced by the temperature ratings of the motor and depends on the material choice and the cooling effort (e.g., conventional air cooling or more complex water cooling). The magnetomotive force, which determines the producible forces, results from the available winding area A_{coil}, the slot fill factor k_{coil}, and the maximum allowed current density $J_{\max}$

$$\Theta_{\max} = J_{\max} \cdot A_{\mathrm{coil}} \cdot k_{\mathrm{coil}}. \tag{1}$$

The slot fill factor was set to 0.5, which corresponds to the value of prototype coils. The winding area itself is a function of several design parameters

$$A_{\mathrm{coil}} = f(q, r_S, \delta_{\mathrm{tt}}, \alpha_t). \tag{2}$$

In order to predict the achievable torque and radial bearing forces (for fixed outer motor dimensions), this maximum allowed current density has to be set as a boundary condition. Moreover, the required magnetic gap thickness has to be determined. It is usually derived from the required application specifications. Additionally, the saturation curve of the iron material has an influence because an energy-dense design with large magnetomotive forces can only be achieved when the iron parts are slightly driven into saturation. However, there is an upper limit because the rotor performance would be reduced drastically for too extensive saturation values. For the remaining design variables, there is mutual interdependence because of these boundary conditions. For higher magnetomotive force (influenced with the winding area for fixed $J_{\max}$ or the permanent-magnet thickness), the iron parts have to be enlarged in order to avoid heavy saturation. The enlargement of the iron parts, however, leads to a reduction of the available space for windings and permanent-magnet material, and it reduces the magnetic gap radius. In the end, an optimal design, where the proportion of iron, winding, and permanent-magnet material is well balanced, can be found. Unfortunately, this setup is only valid if the boundary conditions (maximum allowed current density, magnetic gap thickness, and iron material) stay constant. If there is a change in one of these factors, the optimum has to be determined again.

There are other important design parameters, such as material choice or coil layout (e.g., winding number, shape, and wire diameter). Moreover, the electrical ratings (required power, system voltage, and maximum possible current) have to be chosen at an early design step.

III. DESIGN STUDY FOR THE STATOR TEETH

When looking at the design of the stator teeth together with the tooth tips, very interesting characteristics can be found. There are three main geometric variables that can be varied, namely, the tooth angle α_t, the radial tooth tip length δ_{tt}, and the tooth tip angle α_{tt}. Using 3-D electromagnetic finite element method (FEM) simulations [18], the influence of the tooth shape on the torque and the passive and active bearing forces is investigated.

A. Influence on Torque

Fig. 3 shows the motor torque for three different normalized stator tooth angles ($n_t = 25\%$, 50%, and 75% in (a), (b), and (c), respectively) in dependence on the tooth tip thickness and the tooth tip angle. Moreover, the maximum allowed current density is varied between 5 A/mm^2, which represents an application without any additional cooling (just ambient air), and 15 A/mm^2, which represents an application with additional water cooling of the coils. When enlarging the tooth tip angle, the torque first decreases until it reaches zero and then reverses its direction. This can be explained with the varying flux linkage between the permanent magnets of the rotor and the coils placed on the stator teeth. In the beginning, for small tooth tip angles, the flux linkage per stator tooth (per coil) is generated by a certain permanent magnet. When the tooth tip angle gets enlarged, the flux linkage is additionally influenced by the two adjacent permanent magnets with opposite magnetization directions compared to the one in the middle. At some point (e.g., for a tooth tip ratio n_{tt} in the range of 1.4 as in Fig. 3), the influence of the permanent magnets is balanced, and the net flux linking with the stator coil is zero. For a further angle increase, the flux linkage is dominated by the two outer permanent magnets in the rotor which have opposite magnetization directions compared to the single magnet in between them. Hence, the influence of

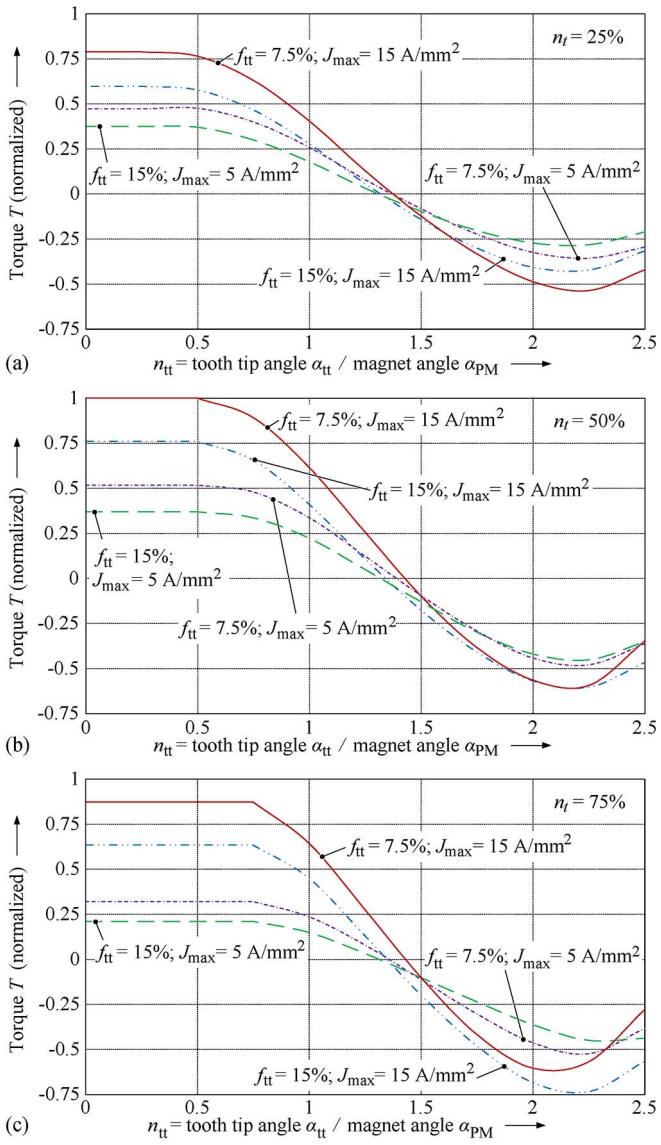

Fig. 3. Influence of the tooth tip angle α_{tt} and the radial tooth tip length δ_{tt} on the torque for two different excitation levels ($J_{\max} = 5$ and 15 A/mm^2) and three different tooth angles ($n_t = 25\%$, 50%, and 75% in (a), (b), and (c), respectively). The torque plots have been normalized with the highest torque value occurring in (b). Note that the design and, consequently, the torque remain constant for all $n_{\mathrm{tt}} \leq n_t$. ($q = 6, p = 8, r_R = 74$ mm, $f_m = 6.75\%$, $f_{\mathrm{PM}} = 8\%$, and $f_{\mathrm{BI}} = 6.75\%$.)

this single magnet in the middle is outweighed by the flux of the outer two, wherefore the net flux direction and the torque direction get reversed. The maximum possible tooth tip ratio n_{tt} is given as the pole number divided by the slot number (2.67 for the topology in Fig. 3).

As a consequence, two design options with either open teeth (small tooth tip angle) or closed teeth (large tooth tip angle) are possible for the generation of sufficient motor torque. Additionally, Fig. 3 reveals that there is a promising tooth angle for open teeth in the range of 50% of the permanent-magnet angle [as in (b)] and that the tooth tips should not exceed a certain thickness, whereas for closed teeth, the tooth angle and the tooth tip thickness should be rather large [as in (c)]. There is a tradeoff between large coil space (small tooth angle), which allows for large magnetomotive force, avoiding iron saturation

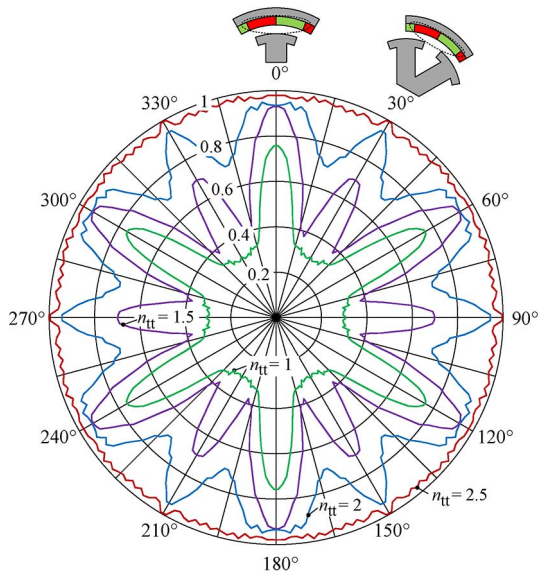

Fig. 4. Influence of the tooth tip angle on the axial force (normalized) acting onto two joining magnets (one pole pair) of the rotor in dependence on the angular position. ($q = 6$, $p = 8$, $r_R = 74$ mm, $f_m = 6.75\%$, $f_{\mathrm{PM}} = 8\%$, $f_{\mathrm{BI}} = 6.75\%$; and $n_t = 50\%$; forces are normalized.)

(large tooth angle), and a favorable flux linkage between the rotor and the stator tooth.

B. Influence on Passive Bearing Forces

The possibility of choosing different ranges for the tooth tip angle is advantageous for the design of the passive magnetic bearing because an important relation holds true for the attracting passive reluctance forces. When the tooth tip angle is increased, larger iron areas are facing the magnets. Consequently, all the passive forces get enlarged. For the axial and the tilting stability, larger reluctance forces are desirable because the bearing stability directly depends on them. In Fig. 4, the axial force action onto two joining magnets (one pole pair) in dependence on the angular rotor position is shown. For small tooth tip angles, there is a large difference whether the pole pair faces the center of a tooth tip (for rotor angles of $0°, 60°, \ldots$) or whether it is in between two stator teeth (for rotor angles of $30°, 90°, \ldots$). This difference vanishes when the tooth tip angle is enlarged. For the overall axial force acting on the rotor (summed up over all magnets), this strong variation for small tooth tip angles smoothens out. Moreover, the total force is obviously larger with an increased tooth tip angle. There is an unavoidable tradeoff between the desired large passive bearing forces in the axial and tilting directions and the passive reluctance forces in the radial directions. The latter pull the rotor out of its center position, and an active control is required to bring the rotor back to the working position. This means that an active bearing has to counteract the destabilizing passive radial forces. In order to decrease the required effort for the active radial bearing, this destabilizing passive force should be small, which is in direct contradiction to the wish for large axial and tilting stability. The mentioned influence of the tooth tip angle on the passive radial force is shown in Fig. 5. The rotor is displaced from its center position, changing the magnetic gap

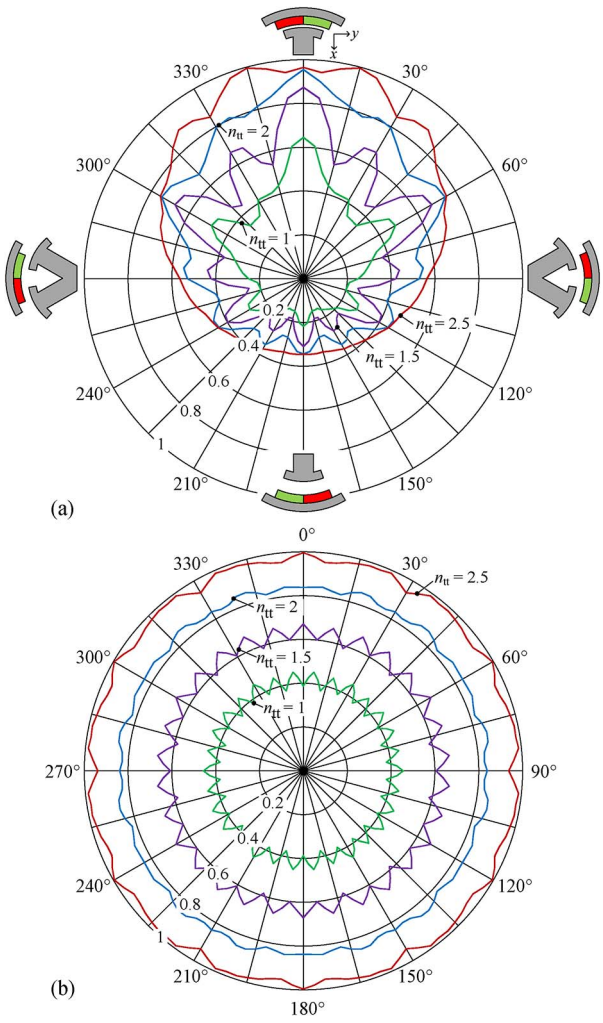

Fig. 5. Destabilizing radial force acting onto two joining magnets (one pole pair) and the back iron ring in (a) and onto the rotor in (b) in dependence on the tooth tip angle and the angular rotor position. The rotor is displaced into the positive x-direction toward the junction of the considered pole pair for an angle of 0°. ($q = 6$, $p = 8$, $r_R = 74$ mm, $f_m = 6.75\%$, $f_{\mathrm{PM}} = 8\%$, $f_{\mathrm{BI}} = 6.75\%$, and $n_t = 50\%$; forces are normalized in (a) and (b) individually.)

in dependence on the rotor angle. In Fig. 5(a), the attracting radial force acting onto these very two magnets (one pole pair; the remaining magnets have been omitted) and the back iron ring is plotted for varying rotor angles with the force measured in the radial direction. The rotor displacement is constant (into the positive x-direction) so that the magnetic gap in between the stator and this magnet pair changes with the rotor angle. In the beginning (at 0°), the magnetic gap is narrow, then increases, and becomes maximal for 180°. The curve would describe a circle if there was no radial displacement (i.e., no change in the magnetic gap). In this case, however, the curve is distorted, as can be seen in Fig. 5(a). Additionally, it can be seen that the forces grow with increased tooth tip angles. Summing up over all rotor magnets, the resulting radial force becomes more or less independent from the rotor angle (see Fig. 5(b), normalized after a rotor displacement into the positive x-direction). Obviously, the total force also becomes larger once the tooth tips are enlarged. From this point of view, smaller

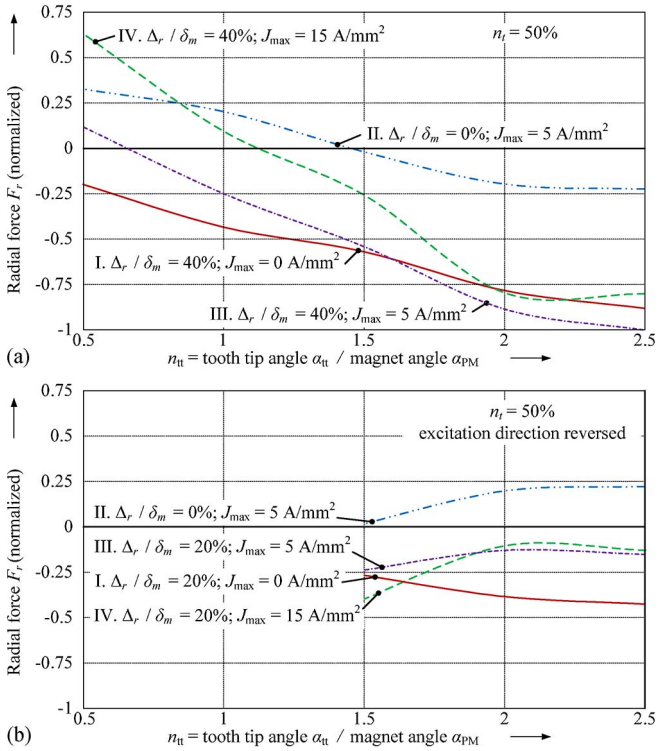

Fig. 6. Active and passive radial bearing forces in dependence on the tooth tip angle for varying radial displacement Δr and coil excitation. ($q = 6$, $p = 8$, $r_R = 74$ mm, $f_m = 6.75\%$, $f_{\mathrm{PM}} = 8\%$, $f_{\mathrm{BI}} = 6.75\%$, and $f_{\mathrm{tt}} = 7.5\%$.)

tooth tips would be favorable for the radial bearing, as discussed before.

C. Influence on Active Radial Bearing

It was shown that the passive radial forces are enlarged when the tooth tip angle is increased. Therefore, it has to be investigated whether the active magnetic bearing in the radial direction can counteract these forces in order to guarantee a stable operation. In Fig. 6(a), the resulting radial force for different radial rotor displacements Δr into the negative x-direction in dependence on the tooth tip angle is shown. Due to stator and rotor encapsulations and the tank wall in between the magnetic gap, the actual fluid gap (which is the operating range that has to be controlled by the bearing) is about 40% of the magnetic gap. If no current is applied to the coils, a negative force results which would displace the rotor even further until it comes to a mechanical touchdown (curve I). Hence, a counterforce (II) has to be generated with the coil system so that the overall force becomes positive again and moves the rotor back into the positive x-direction toward its center position (III and IV). Fig. 6(a) further reveals that the rotor can be stabilized for $n_{\mathrm{tt}} < 65\%$ in case of low excitation with 5 A/mm^2 or up to $n_{\mathrm{tt}} < 110\%$ if high excitation (15 A/mm^2) is applied.

For larger tooth tip angles (beyond 150%), the active radial force (II) is reversed for the same excitation (for the same reason as for the torque), and the bearing would just support the displacement instead of counteracting it. Therefore, the excitation has been reversed in Fig. 6(b) for closed stator teeth.

It can be seen that the active force (II) becomes positive and it is counteracting the destabilizing passive one (I). However, the resulting total force (III and IV) never becomes positive which means that the destabilizing passive radial force is dominant even for a displacement of only 20% in relation to the entire magnetic gap. Moreover, even for high excitation (IV, with 15 A/mm^2), the active bearing cannot cope with the destabilization. In fact, the difference between moderate excitation (III, with 5 A/mm^2) and high excitation is very small which means that there is almost no gain anymore for the active force when the excitation is increased. This is an indicator that the iron material is heavily driven into saturation. As in the case of the torque, the tooth tip thickness δ_{tt} could be enlarged to decrease the saturation level. However, this also decreases the available winding area and, consequently, the applicable magnetomotive force.

D. Open Versus Closed Teeth

In the previous sections, it was found that there generally exist two possibilities to design the stator teeth. They can either be open, with the tooth tip angle in the range of the tooth angle itself, or closed with rather large tooth tip angles. Both alternatives could produce sufficient torque, whereas closed teeth would be beneficial for the passive magnetic bearing. For the active magnetic bearing, however, a stable implementation with closed teeth is hardly achievable for the required working range. Therefore, a setup with open stator teeth has to be recommended for this type of bearingless motors and the intended applications. In order to decrease the system complexity, the tooth tips could even be omitted, leading to bar-shaped stator teeth. This measure would allow for less costly manufacturing of the stator, and the coils and would simplify some of the assembly steps. In the analysis, this simply corresponds to setting $n_{\mathrm{tt}} = n_t$.

IV. Verification With Test Setup

A prototype setup has been realized in order to confirm the simulation results and to test the motor in a practical manner. The dimensions of this prototype are listed in Table II and correspond to the motor described in [12]. The stator with the concentrated coils is depicted in Fig. 7(a). It can be seen that the tooth tips have been omitted, following the design considerations elaborated before. The stator and the sensor system (for radial and angular position measurements) are then placed below a stainless steel cup [see Fig. 7(b)]. This cup represents the tank indentation so that a real application situation can be tested. The rotor ring (back iron and permanent magnets) levitates around the buried motor.

The torque characteristics of the prototype motor have both been simulated and measured. The achievable torque in dependence on the maximum allowed current density in the coils is plotted in Fig. 8. A convincing accordance between simulation results (solid line) and the measurements (dots) can be found, which confirms the correctness of the simulation results and, consequently, the design analysis presented in this paper.

TABLE II
Prototype Dimensions

Parameter	Symbol	Value
Stator slot number	q	6
Pole pair number	p	8
Outer rotor diameter	r_R	74 mm
Maximum allowed current density	$J_{\max}$	5 / 15 A/mm^2
Magnetic gap length	δ_m	5 mm
Permanent magnet thickness	δ_{PM}	6 mm
Back iron thickness	δ_{BI}	5 mm
Relative stator tooth angle	n_t	66 %
Motor height	l	45 mm
Stator radius	r_S	58 mm
Slot fill factor	k_{coil}	0.5
Number of windings / coil	n_{coil}	300
Rotor weight	m_R	1.8 kg

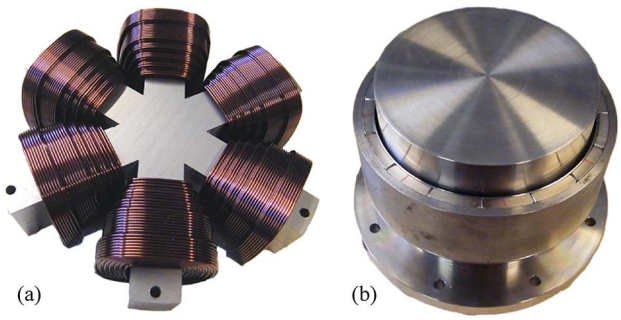

Fig. 7. Stator in (a), which consists of six concentrated coils (one per stator tooth), is placed below a stainless steel cup in (b). For this prototype, the cup represents the tank indentation. The rotor ring is placed around the tank indentation (see also Fig. 1).

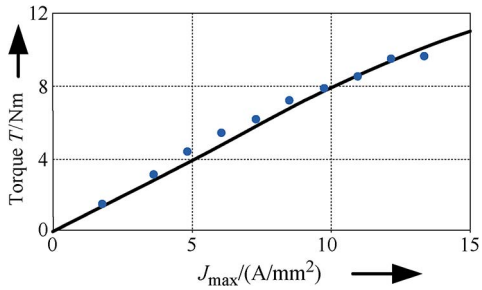

Fig. 8. Comparison of (solid line) simulation results and (dots) measurements of the torque characteristics on the prototype in dependence on the maximum allowed current density in the coils.

Additionally, a test run with an experimental tank setup has been undertaken, and the corresponding measurements are presented in Fig. 9. In the beginning, the rotor (with mixing head) is levitated and turns with 100 r/min inside water.

During the test, it is accelerated to 280 r/min (which was found to be a reasonable mixing speed for this test setup) and decelerated back to 100 r/min again. The radial positions (split into x- and y-directions) are permanently measured during the whole experiment. It can be seen that the radial rotor is kept

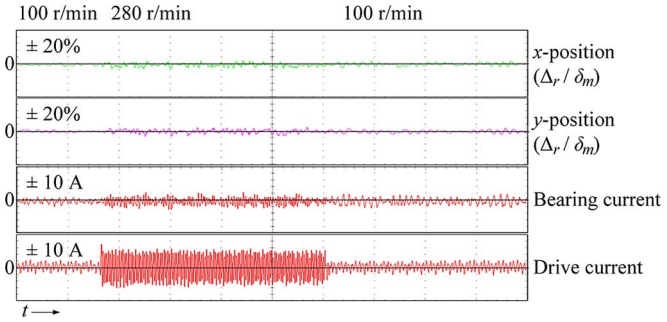

Fig. 9. Measurements of the radial positions and the bearing and drive current in one phase using the prototype motor inside a test tank filled with water. The rotor is levitated and spinning with 100 r/min, accelerated to 280 r/min and decelerated back to 100 r/min.

in the center position with high accuracy during the entire test run. Additionally, the drive and bearing current of one phase is determined. The latter reveals that only little current is needed for a stable control of the magnetic bearing. The drive current is rather small for the lower speed. Once it is running with 280 r/min, however, the water flow becomes turbulent, and a rather large torque is required to overcome the water resistance. Consequently, the current increases in order to provide the mixing torque.

As can be seen in Table II, the relative stator tooth angle n_t was set to 66% for this prototype. This is a compromise, as it lowers the achievable torque and active radial force but enhances the stiffness of the passive bearings in the axial and tilting directions. The axial stiffness has to be sufficiently large to counteract the rotor weight. For this prototype setup, the rotor gets lowered 5 mm in relation to the stator until a force balance is reached. Nevertheless, this axial rotor position is acceptable compared to the total motor height of 45 mm. Additionally, the design of the mixing blades has to be considered. Ideally, a mixing stream should be created which further lifts the rotor and supports the axial stiffness. During the experiments, the rotor was levitated in a stable manner in all degrees of freedom.

V. Conclusion

A general design study for bearingless motors in exterior rotor construction has been presented. The important design parameters have been listed, and their interconnections were explained. For the stator, it was shown that the teeth can either be open (small tooth tip angle) or closed (large tooth tip angle) for both torque and passive bearing forces. For the active radial bearing, however, a design implementation with open teeth is clearly recommended. Therefore, the suggestion is to omit the tooth tips and to use bar-shaped stator teeth.

References

[1] T. Schneeberger, T. Nussbaumer, and J. W. Kolar, "Magnetically levitated homopolar hollow-shaft motor," *IEEE/ASME Trans. Mechatronics*, vol. 15, no. 1, pp. 97–107, Feb. 2010.

[2] W. Gruber, T. Nussbaumer, H. Grabner, and W. Amrhein, "Wide air gap and large-scale bearingless segment motor with six stator elements," *IEEE Trans. Magn.*, vol. 46, no. 6, pp. 2438–2441, Jun. 2010.

[3] G. Catapano, P. Czermak, R. Eibl, D. Eibl, and R. Pörtner, "Bioreactor design and scale-up," in *Cell and Tissue Reaction Engineering: Principles and Practice,* 1st ed. Berlin, Germany: Springer-Verlag, 2009, pp. 173–259.

[4] M. Ooshima and C. Takeuchi, "Magnetic suspension performance of a bearingless brushless dc motor for small liquid pumps," *IEEE Trans. Ind. Appl.*, vol. 47, no. 1, pp. 72–78, Jan./Feb. 2011.

[5] F. Zürcher, T. Nussbaumer, W. Gruber, and J. W. Kolar, "Design and development of a 26-pole and 24-slot bearingless motor," *IEEE Trans. Magn.*, vol. 45, no. 10, pp. 4594–4597, Oct. 2009.

[6] W. Gruber, W. Amrhein, and M. Haslmayr, "Bearingless segment motor with five stator elements: Design and optimization," *IEEE Trans. Ind. Appl.*, vol. 45, no. 4, pp. 1301–1308, Jul./Aug. 2009.

[7] Y. Asano, A. Mizuguchi, M. Amada, J. Asama, A. Chiba, M. Ooshima, M. Takemoto, T. Fukao, O. Ichikawa, and D. G. Dorrell, "Development of a four-axis actively controlled consequent-pole-type bearingless motor," *IEEE Trans. Ind. Appl.*, vol. 45, no. 4, pp. 1378–1386, Jul./Aug. 2009.

[8] S. Silber, W. Amrhein, P. Boesch, R. Schoeb, and N. Barletta, "Design aspects of bearingless slice motors," *IEEE/ASME Trans. Mechatronics*, vol. 10, no. 6, pp. 611–617, Dec. 2005.

[9] M. Ooshima, A. Chiba, T. Fukao, and M. A. Rahman, "Design and analysis of permanent magnet-type bearingless motors," *IEEE Trans. Ind. Electron.*, vol. 43, no. 2, pp. 292–299, Apr. 1996.

[10] Y. Christi and M. Moo-Young, "Clean-in-place systems for industrial bioreactors: Design, validation and operation," *J. Ind. Microbiol. Biotechnol.*, vol. 13, no. 4, pp. 201–207, Jul. 1994.

[11] T. Yamada, Y. Nakano, J. Asama, A. Chiba, T. Fukao, T. Hoshino, and A. Nakajima, "Outer rotor consequent-pole bearingless motor with improved start-up characteristics," *IEEE Trans. Magn.*, vol. 44, no. 11, pp. 4273–4276, Nov. 2008.

[12] M. Nakagawa, Y. Asano, A. Mizuguchi, A. Chiba, C. X. Xuan, M. Ooshima, M. Takemoto, T. Fukao, O. Ichikawa, and D. G. Dorrell, "Optimization of stator design in a consequent-pole type bearingless motor considering magnetic suspension characteristics," *IEEE Trans. Magn.*, vol. 42, no. 10, pp. 3422–3424, Oct. 2006.

[13] H. Sugimoto, K. Kamiya, R. Nakamura, J. Asama, A. Chiba, and T. Fukao, "Design and basic characteristics of multi-consequent-pole bearingless motor with bi-tooth main poles," *IEEE Trans. Magn.*, vol. 45, no. 6, pp. 2791–2794, Jun. 2009.

[14] T. Reichert, T. Nussbaumer, W. Gruber, and J. W. Kolar, "Bearingless permanent-magnet motor with 4/12 slot-pole ratio for bioreactor stirring applications," *IEEE/ASME Trans. Mechatronics*, vol. 16, no. 3, pp. 431–439, Jun. 2011.

[15] T. Reichert, T. Nussbaumer, and J. W. Kolar, "Novel bearingless brushless motor in exterior rotor construction for stirred bioreactors," in *Proc. 5th IET Int. Conf. PEMD*, Brighton, U.K., Apr. 2010, pp. 1–6.

[16] T. Reichert, T. Nussbaumer, and J. W. Kolar, "Bearingless 300-W PMSM for bioreactor mixing," *IEEE Trans. Ind. Electron.*, vol. 59, no. 3, pp. 1376–1388, Mar. 2012.

[17] B. Warberger, R. Kaelin, T. Nussbaumer, and J. W. Kolar, "50-Nm/2500-W bearingless motor for high-purity pharmaceutical mixing," *IEEE Trans. Ind. Electron.*, vol. 59, no. 5, pp. 2236–2247, May 2012.

[18] Maxwell 3D, 2011. [Online]. Available: http://ansoft.com/products/em/maxwell/

Thomas Reichert (S'09) was born in Schaffhausen, Switzerland, in 1983. He received the M.Sc. degree in electrical engineering and information technology from the Swiss Federal Institute of Technology (ETH) Zurich, Zurich, Switzerland, in 2008. The focus during his studies was on mechatronics, robotics, power systems, and control. During his Master's thesis, he simulated rotor dynamics and implemented a magnetic bearing for a megaspeed drive. Since October 2008, he has been working toward the Ph.D. degree in the Power Electronic Systems Laboratory, ETH Zurich, where he is working on high-torque magnetically levitated motors.

Johann W. Kolar (F'10) received the M.Sc. and Ph.D. degrees (*summa cum laude/promotio sub auspiciis praesidentis rei publicae*) from the University of Technology Vienna, Vienna, Austria.

Since 1984, he has been working as an independent international consultant in close collaboration with the University of Technology Vienna in the fields of power electronics, industrial electronics, and high-performance drives. He has proposed numerous novel converter topologies and modulation/control concepts, e.g., the VIENNA Rectifier, the Swiss Rectifier, and the three-phase ac–ac sparse matrix converter. He has published over 450 scientific papers in international journals and conference proceedings and has filed more than 85 patents. He was appointed Professor and Head of the Power Electronic Systems Laboratory at the Swiss Federal Institute of Technology (ETH) Zurich, Zurich, Switzerland, on February 1, 2001. The focus of his current research is on ac–ac and ac–dc converter topologies with low effects on the mains, e.g., for data centers, more electric aircraft, and distributed renewable energy systems, and on solid-state transformers for smart microgrid systems. Further main research areas are the realization of ultracompact and ultraefficient converter modules employing latest power semiconductor technology (SiC and GaN), micro power electronics and/or power supplies on chip, multidomain/scale modeling/simulation and multiobjective optimization, physical model-based lifetime prediction, pulsed power, and ultrahigh-speed and bearingless motors.

Dr. Kolar is a member of the Institute of Electrical Engineers of Japan (IEEJ) and of the International Steering Committees and Technical Program Committees of numerous international conferences in the field (e.g., Director of the Power Quality Branch of the International Conference on Power Conversion and Intelligent Motion). He is the founding Chairman of the IEEE Power Electronics Society (PELS) Austria and Switzerland Chapter and the Chairman of the Education Chapter of the EPE Association. He served as an Associate Editor of the IEEE TRANSACTIONS ON INDUSTRIAL ELECTRONICS from 1997 to 2000 and has served as an Associate Editor of the IEEE TRANSACTIONS ON POWER ELECTRONICS since 2001. Since 2002, he has also been an Associate Editor of the *Journal of Power Electronics* of the Korean Institute of Power Electronics and a member of the Editorial Advisory Board of the *IEEJ Transactions on Electrical and Electronic Engineering*. He was the recipient of the Best Transactions Paper Award of the IEEE Industrial Electronics Society in 2005, the Best Paper Award of the ICPE in 2007, the 1st Prize Paper Award of the IEEE Industry Applications Society Industrial Power Converter Committee in 2008, the IEEE IECON Best Paper Award of the IES PETC in 2009, the IEEE PELS Transaction Prize Paper Award 2009, the Best Paper Award of the IEEE/ASME TRANSACTIONS ON MECHATRONICS 2010, the IEEE PELS Transactions Prize Paper Award 2010, the Best Paper 1st Prize Award at the ECCE Asia 2011, and the 1st Place IEEE IAS Society Prize Paper Award 2011. Furthermore, he was the recipient of the ETH Zurich Golden Owl Award 2011 for excellent teaching. He also received an Erskine Fellowship from the University of Canterbury, Christchurch, New Zealand, in 2003. He initiated and/or is the founder/cofounder of four spin-off companies targeting ultrahigh-speed drives, multidomain/level simulation, ultracompact/efficient converter systems, and pulsed power/electronic energy processing. In 2006, the European Power Supplies Manufacturers Association recognized the Power Electronics Systems Laboratory of ETH Zurich as the leading academic research institution in power electronics in Europe.

Thomas Nussbaumer (S'02–M'06) was born in Vienna, Austria, in 1975. He received the M.Sc. degree (with honors) in electrical engineering from the University of Technology Vienna, Vienna, in 2001 and the Ph.D. degree from the Power Electronic Systems (PES) Laboratory, Swiss Federal Institute of Technology (ETH) Zurich, Zurich, Switzerland, in 2004.

From 2001 to 2006, he was with the PES Laboratory, where he conducted research on the modeling, design, and control of three-phase rectifiers, power factor correction techniques, and electromagnetic compatibility. Since 2006, he has been with Levitronix GmbH, Zurich, Switzerland, where he is currently working on bearingless motors, magnetic levitation, and permanent-magnet motor drives for the semiconductor and biotechnology industry. His current research is focused on compact and high-performance mechatronic systems, including novel power electronics topologies, control techniques, drive systems, sensor technologies, electromagnetic interference, and thermal aspects.